Rapid development of spiral garnets during subduction zone metamorphism revealed from high-resolution Sm-Nd garnet geochronology

Thomas P. Farrell[1,2,*], Domingo Aerden[3], Ethan F. Baxter[1], Paul G. Starr[1], and Mike L. Williams[4]

[1]Department of Earth and Environmental Sciences, Boston College, Chestnut Hill, Massachusetts 02467, USA
[2]Department of Geosciences, Boise State University, Boise, Idaho 83702, USA
[3]Departamento de Geodinámica, Universidad de Granada, 18071 Granada, Spain
[4]Department of Geosciences, University of Massachusetts, Amherst, Massachusetts 01003, USA

ABSTRACT

Multiple studies have applied zoned garnet geochronology to place temporal constraints on the rates of metamorphism and deformation during orogenesis. We report new high-resolution isotope dilution–thermal ionization mass spectrometry Sm-Nd isochron ages on concentric growth zones from microstructurally and thermodynamically characterized garnets from the Betic Cordillera, southern Spain. Our ages for the garnet core (13.64 ± 0.31 Ma), mantle (13.41 ± 0.37 Ma), and rim (13.34 ± 0.45 Ma) indicate rapid garnet growth and are consistent with published garnet ages interpreted to reflect high-pressure metamorphism in the region. Thermodynamic analysis indicates garnets grew during subduction at ~1.5–2.0 GPa and 570–600 °C. The core to rim duration of spiral garnet growth was just a few hundred thousand years. While other zoned garnet studies have shown similar rapid growth in subduction zone settings, this is the first documentation of such rapid growth of a spiral garnet. Combining this garnet growth duration with the magnitude of spiral inclusion trail curvature, we compute a strain rate of $\sim 10^{-13}$ s^{-1}, an order of magnitude faster than all previous spiral garnet studies. We interpret that these spiral garnets recorded a rapid pulse of deformation and strain during the final stages of subduction and incipient exhumation.

INTRODUCTION

The abundance of garnet in metamorphic rocks, in combination with its ability to grow in a wide-range of pressure, temperature, and deformational (*P-T-D*) conditions and to be directly dated, has made it a primary target for investigating tectonometamorphic processes (Baxter and Scherer, 2013). The physical and chemical resistance of garnet to syn- and postgrowth alteration allows it to record and preserve information about its earliest growth stages. Commonly zoned both compositionally and texturally, garnet can provide a near-continuous history of evolving *P-T-D* conditions. A spectacular example of textural zoning is the development of spiral inclusion trails (Fig. 1A), which form when garnet overgrows an actively evolving matrix foliation during deformation. Spiral trails have been interpreted to

form either from syntectonic rotation of the garnet crystal (Rosenfeld, 1968) or from growth over a curved foliation without rotation (Bell, 1985). Here we use "spiral garnet" merely to describe the observed texture with no definitive conclusion toward either model. Either way, spiral garnet provides a critical constraint on the rates of metamorphic mineral growth and deformation during tectonism. Strain rates across orogenic belts have been estimated to be $\sim 10^{-14}$ s^{-1}; however, large spatial and temporal variations have been shown, reflecting the localization of strain at different length scales (Pfiffner and Ramsay, 1982; Fagereng and Biggs, 2019). Direct strain rate determinations that combine geochronology and strain data on the same rock are scarce. Christensen et al. (1989, 1994), and Vance and O'Nions (1992) were among the first to employ zoned garnet geochronology to place direct temporal constraints on the rate and duration of garnet growth and link them to the rates of metamorphism and deformation. These early studies reported garnet

developing on multi-million-year time scales during regional metamorphism. More recent work on subducted lithologies (Dragovic et al., 2015; Tual et al., 2022) have shown evidence for rapid pulses of garnet growth, on the order of <1 m.y. Prior to our study, Christensen et al. (1989, 1994) and Vance and O'Nions (1992) were the only studies to use zoned garnet geochronology on spiral garnets to calculate a strain rate. Their findings documented strain rates of $\sim 10^{-14}$ s^{-1} during regional metamorphism, consistent with other constraints on regional metamorphic strain rates (Pfiffner and Ramsey, 1982; Müller et al., 2000; Baxter and DePaolo, 2004). To investigate the rates of metamorphism and deformation in the subducted lithologies of the Betic Cordillera, we applied detailed microstructural analysis, thermobarometry, and high-resolution zoned Sm-Nd garnet geochronology to garnets hosting spectacular spiral inclusion trails. The results show very rapid garnet growth and fabric evolution (Fig. 1A).

GEOLOGIC SETTING

The Betic Cordillera is located at the western termination of the Mediterranean-Alpine orogenic system (Platt et al., 2013). Its metamorphic hinterland, the Alborán Domain, is composed of three nappe complexes, the lowest of which is the Nevado-Filábride Complex (NFC), from which the spiral garnet-bearing samples from this study were collected. The NFC outcrops as a tectonic window in the central and eastern Betics where it forms a broadly east-west–trending anticlinorium including the Sierra Nevada and Sierra de los Filabrides mountains. The NFC has been subdivided into the lower Veleta Complex composed of polymetamorphic Paleozoic graphite schists and quartzites. The overlying Mulhacén Complex (MC) contains similar

Thomas P. Farrell 🆔 https://orcid.org/0000-0002-6277-4533
*thomasfarrell@u.boisestate.edu
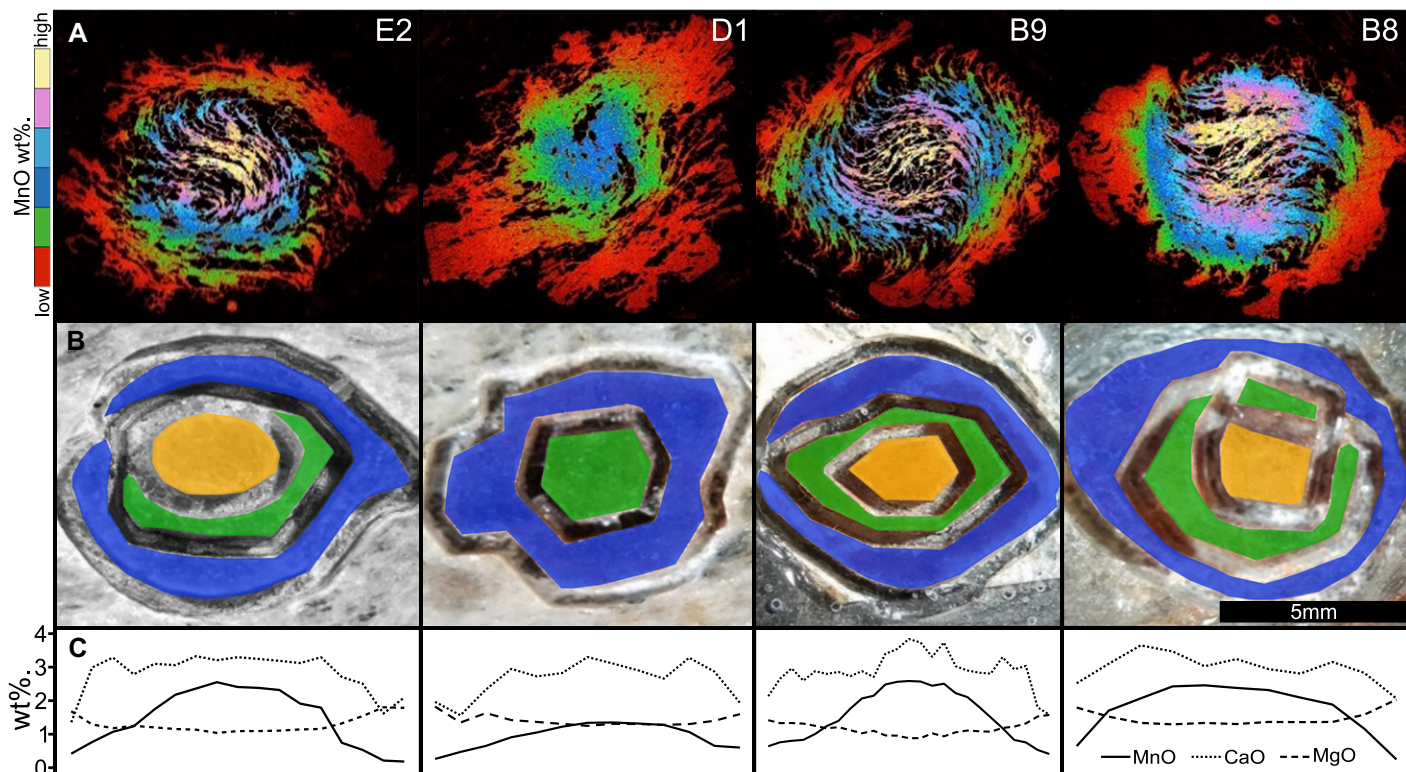
Figure 1. (A) Electron microprobe maps of MnO concentration used to determine individual garnet growth zones for micro-drilling. MnO wt% ranged from 0.254 to 2.585. (B) Photographs of garnets after micro-drilling; zones based upon Mn concentrations and inclusion trail geometry. Three growth zones were determined: cores—yellow; mantles—green; rims—blue. (C) Microprobe major element transects; solid—MnO; dashed—MgO; dotted—CaO.

Paleozoic basement rocks overlain by a Permian–Triassic, and possibly younger, metasedimentary sequences. From bottom to top, they are composed of micaschists, calcschists, and marbles (Puga et al., 2002). Eclogitized mafic and ultramafic lenses within this cover sequence have been interpreted as remains of a narrow branch of the Alpine Tethys (Puga et al., 2011) that originally separated the Iberian paleomargin (including most of the NFC) from a microcontinent that lay to the east and included the overlying Alpujárride and Maláguide Complexes (Platt et al., 2013). The high-pressure lithologies were subducted to pressure of 1.5–2.0 GPa at 20−13 Ma (Sánchez-Vizcaíno et al., 2001; Platt et al., 2006; Kirchner et al., 2016). Exhumation, including low-pressure–high-temperature metamorphic overprinting, commenced as early as 15–13 Ma (Santamaría-López et al., 2019). Recent work by Aerden et al. (2022) illuminated the spiral garnet sample of focus in our study from the MC as a relic from the end of the ca. 13 Ma high-pressure event.

MICROSTRUCTURE AND THERMOBAROMETRY

Sample 27.1.2 is a metapelite with a mineral assemblage of kyanite (Ky), chloritoid (Ctd), garnet (Gt), phengite (Ph), paragonite (Pg), and quartz (Qtz) with minor amounts of rutile (Ru), ilmenite (Ilm), and apatite (Ap). The abundant centimeter-sized almandine garnets contain abundant inclusions ($\sim$50% by volume) of Qtz, Ph, Ctd, and large Ky inclusions within the rims. There is no textural or mineralogical evidence of retrograde overprinting of the stable Ky-Ctd-Gt-Ph-Pg assemblage. Peak pressure-temperature conditions were constrained to $\sim$1.5–2.0 GPa and $\sim$570–600 °C based on the stability of the characteristic high-pressure Gt-Ctd-Ky peak assemblage and the elevated Si concentration of white mica inclusions within garnet and in the matrix (Si = 3.19–3.24 cations per formula unit; Fig. 2). In addition, these peak pressures are consistent with previous estimates for the MC, derived from the associated mafic eclogite bodies (1.5–2.2 GPa; Platt et al., 2006; Puga et al., 2011), from garnet schists of the NFC (2.0–2.2 GPa; Santamaría-López et al., 2019), and for similar Gt-Ctd-Ky schists in the Betics (Smye et al., 2010). Lower pressures (0.4–0.8 GPa) documented in other studies of the NFC (Aerden et al., 2013; Santamaría-López et al., 2019) represent overprinting during exhumation not observed in the rocks of our study. The three-dimensional geometry of the spiral inclusion trails in garnet were characterized using the asymmetry technique of Hayward (1990), with multiple vertical and horizontal cuts of the oriented sample. The inclusion trails spiral up to $\sim$222° with subhorizontal spiral-axes trending predominantly east-west.

GARNET GEOCHRONOLOGY
Methods

Preliminary bulk garnet geochronology using isotope dilution–thermal ionization mass spectrometry (ID-TIMS) gave a date of 13.62 ± 0.69 Ma (Aerden et al., 2022). This date agrees with the lower bound of Lu-Hf garnet ages of 18.2–13.3 Ma (Platt et al., 2006) and Rb-Sr multiphase ages of 20.1–13.3 Ma (Kirchner et al., 2016) from the MC. From the same sample, four $\sim$1 cm garnets, with representative inclusion trails, were selected for zoned Sm-Nd geochronology. Using Mn concentration and inclusion trail geometries as proxies for garnet growth, we selected three growth zones for garnets B9, E2, and B8, and two growth zones for garnet D1 (Fig. 1B) for micro-sampling, following the procedures of Pollington and Baxter (2011). Due to small sample size, core and mantle zones from B9, E2, and B8 and rims from B9 and B8 were combined. The six separates were crushed, hand-picked, and sieved to form a coarse garnet separate and a garnet powder separate. The resulting 12 separates were put through a partial dissolution procedure consisting of alternating HF and HNO₃ steps to dissolve out contaminating inclusions following the methods of Starr et al. (2020).

Results

The eight garnet analyses included on the isochrons (see Table S2 in the Supplemental
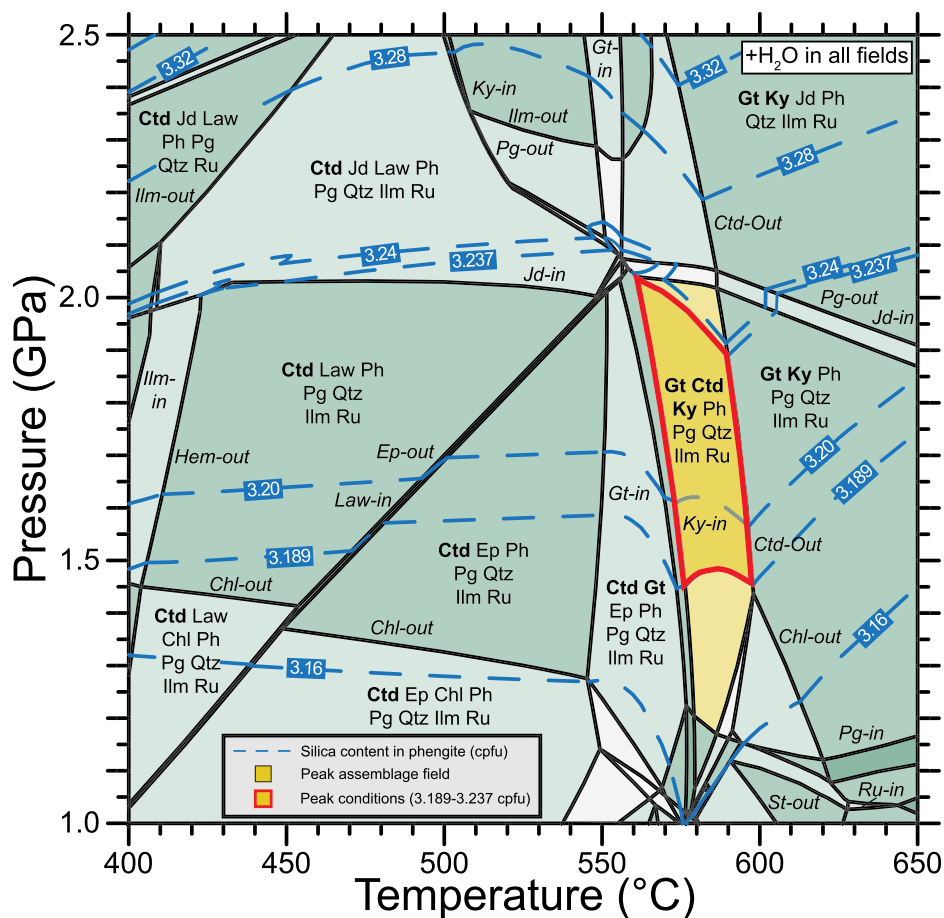
Figure 2. Pseudosection for sample 27.1.2 [MnO-Na₂O-CaO-K₂O-FeO-MgO-Al₂O₃-SiO₂-H₂O-TiO₂-Fe₂O₃, water in excess, X-ray fluorescence bulk composition: 27% ferric iron content] from the Betic Cordillera, southern Spain. Silica content in phengite isopleths (cations per formula units: cpfu) are plotted as blue dashed lines. The peak conditions (red outlined area) are calculated based on peak assemblage stability and the range of maximum silica contents observed in different phengite grains included within the garnet and the matrix (Si = 3.19–3.24). See Supplemental Material (see text footnote 1) for all mineral abbreviations and more detailed methods and discussion.

Material[1] for all data) yielded $^{147}Sm/^{144}Nd$ ratios from 1 to 3.9, indicating the successful removal of problematic inclusions (Baxter and Scherer, 2013). Four garnet analyses were rejected due to low $^{147}Sm/^{144}Nd$ ratios (<0.3) and poor run behavior. All zones are paired with a whole rock and four matrix separates from which it is assumed the garnets grew in isotopic equilibrium. We include multiple matrix samples to account for possible matrix heterogeneity, which can affect the age (e.g., Gatewood et al., 2015). Figure 3 shows isochrons for each zone analyzed. Sm-Nd isochron dates were calculated using IsoplotR (Vermeesch, 2018), and errors are reported at 2σ. Zones yielded ID-TIMS dates

of 13.64 ± 0.31 Ma (cores), 13.41 ± 0.37 Ma (mantles), and 13.34 ± 0.45 Ma (rims).

DISCUSSION
**Duration of Garnet Growth**

We interpret these new dates to be the ages of core, mantle, and rim growth. Simply taking the difference in age between the core and rim (while ignoring the mantle age) results in a duration of 0.30 ± 0.54 m.y. (2σ). From this, we can constrain the duration of spiral garnet growth to 0.84 m.y. (2σ maximum) to instantaneous. In fact, plotting all data from core, mantle, and rim on a single isochron reveals a combined age of 13.53 ± 0.23 Ma (mean square of weighted deviates = 1.1) which indicates, once again, a very short duration of growth. Alternatively, we can utilize the statistical value of the mantle age and re-compute a duration using a Bayesian statistical model that requires the simple geometric constraint of core to mantle to rim growth (see the Supplemental Material for details). This analysis yields a most probable

duration of $0.46^{+0.46}_{-0.34}$ m.y. 95% credible interval (c.i.). Regardless of the approach taken, our data confirm very rapid growth of these spiral garnets. While other zoned garnet geochronology studies have shown similar rapid rates of garnet growth in subducted terranes (Pollington and Baxter, 2011; Dragovic et al., 2015; Tual et al., 2022), this is the first documentation of such rapid growth in fully developed spiral garnets.

Given the high precision of these ages, it is worth considering second-order effects that may alter growth age accuracy, such as diffusional resetting or open system rare earth element (REE) mobility. For garnets of this size (~1 cm) and peak temperatures <600 °C, there will be negligible postgrowth diffusional modification of the outermost rim (e.g., Baxter and Scherer, 2013), which would only serve to make the duration shorter. Open system modification of matrix Sm and Nd content during garnet growth (which could alter apparent ages) is also unlikely given limited solubility of REEs in typical crustal fluids (e.g., Baxter and DePaolo, 2002), lack of evidence for advective flow (i.e., veins), and the fact that all garnet, whole rock, and matrix analyses lie on a tight isochron. These effects do not alter the main conclusion that these spiral garnets grew in just a few hundred thousand years.

Strain Rate

Whether the observed spiral garnets from the NFC developed by rotation or non-rotation, the development occurred on a rapid time scale spanning just a few hundred thousand years. Christensen et al. (1989, 1994) and Vance and O'Nions (1992) applied zoned garnet geochronology to calculate shear-strain rates from spiral garnet assuming the model of a spherical garnet rotating in a simple shear flow. The shear-strain rates they obtained were $2.4^{+1.6}_{-0.7} \times 10^{-14}$ s^{-1}, $2.7^{+1.2}_{-0.7} \times 10^{-14}$ s^{-1}, and $1.9 \pm 0.9 \times 10^{-14}$ s^{-1}, respectively. Adopting the same kinematic model as the previous authors, Biermeier and Stüwe (2003) and Berg et al. (2013) calculated average shear-strain rates of $\sim$6.6 $\times 10^{-14}$ s^{-1} and $\sim$4.0 $\times 10^{-14}$ s^{-1}, respectively. These two latter studies do not directly date the duration of garnet growth, but rather use thermodynamic modeling under the assumption of reasonable regional heating rates to estimate the duration of garnet growth. Following the same approach with our spiral garnets (with ~222° inclusion trail curvature observed in sections cut normal to the spiral axis) and our modeled garnet growth duration ($0.46^{+0.46}_{-0.12}$ m.y.), we obtain a most probable strain rate of $1.4^{+4.0}_{-0.7} \times 10^{-13}$ s^{-1} (95% c.i.). This strain rate is an order of magnitude faster than that found in the studies noted above and those determined from methods such as those of Müller et al. (2000) and Pfiffner and Ramsay (1982). Aerden and Ruiz-Fuentes (2020) analyzed spiral garnet from the same
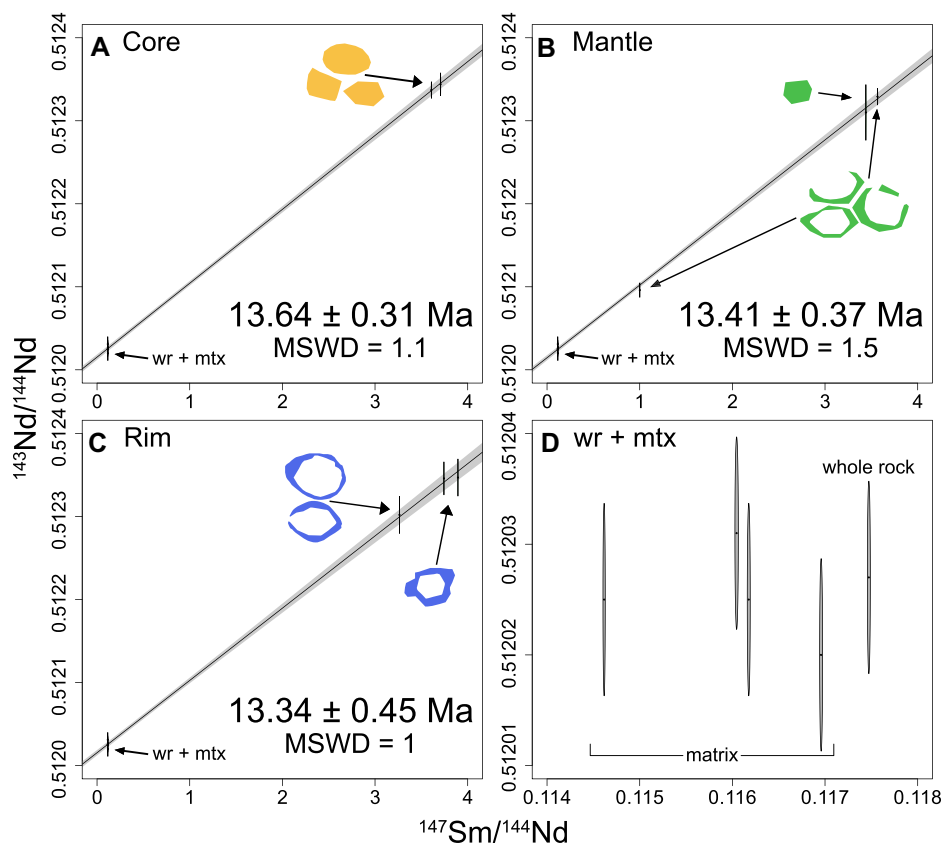
Figure 3. (A–C) Sm-Nd isochrons for core, mantle, and rim zones within garnets from sample 27.1.2 from the Betic Cordillera, southern Spain. Individual garnets and growth zones are as shown in Figure 1. (D) Close-up of the whole rock (wr) and four matrix (mtx) points used in each isochron. MSWD—mean square of weighted deviates.

In the figure panels:
- **A Core**: 13.64 ± 0.31 Ma, MSWD = 1.1, wr + mtx
- **B Mantle**: 13.41 ± 0.37 Ma, MSWD = 1.5, wr + mtx
- **C Rim**: 13.34 ± 0.45 Ma, MSWD = 1, wr + mtx
- **D wr + mtx**: whole rock, matrix

Axes: $^{143}Nd/^{144}Nd$ (vertical), $^{147}Sm/^{144}Nd$ (horizontal)

outcrop as the garnets described herein and argued that they formed by sequential overgrowth of three crenulation cleavages developed alternately with subvertical and subhorizontal orientations without causing significant garnet rotation (Bell, 1985). This model would also explain why spiral-axes are subparallel to the regional mineral lineation (Aerden et al., 2013), instead of perpendicular as expected in the case of simple shear flow. Berg et al. (2013) also considered a "non-rotational" origin of spiral garnets from the Alps as an alternative possibility to simple shear. Assuming 60% shortening associated with each overgrown crenulation cleavage, Berg et al. (2013) calculated an average strain rate of 8×10^{-15} s^{-1}, which is slower by a factor of five compared to the value they obtained for the case of simple shear (4×10^{-14} s^{-1}). The same approach applied to our NFC spiral garnets, assuming overgrowth of three orthogonal crenulation cleavages, yields a most probable strain rate of $1.9^{+5.4}_{-0.9} \times 10^{-13}$ s^{-1} (95% c.i.), which is statistically equivalent to the case of simple shear described above. Regardless of the calculation approach, the spiral garnets in our study record strain rates at least an order of magnitude faster than any other earlier spiral garnet study. Such rapid strain rates have

been documented in faults and shear zones, especially over short length scales (Fagereng and Biggs, 2019). Though less likely, our data allow for near instantaneous garnet growth, which would result in strain rates faster than 5.4×10^{-13} s^{-1} (rotation) and 7.3×10^{-13} s^{-1} (non-rotation), the upper limit of the 95% c.i.

Exhumation Rate

Our thermodynamic modeling suggests that the dated spiral garnets were located at a depth of at least 40 km (∼1.5 GPa), as they stopped growing shortly after ca. 13.34 Ma (rim age). While they do overlap statistically, slightly younger allanite U-Pb ages of 12.87 ± 3.31 Ma to 12.40 ± 4.19 Ma obtained by Santamaría-López et al. (2019) from the MC linked to late-stage garnet growth at pressures of 0.7 GPa (∼20 km). This implies a minimum exhumation rate on the order of 1–4 cm/yr, similar to exhumation rates deduced in HP-LT rocks by Rubatto and Hermann (2001) and Grujic et al. (2011). The garnet growth in this sample likely spans a rapid shift from burial to exhumation within a localized shear zone.

CONCLUSIONS

The rapid time scale over which these spiral garnets formed is the novel result of our study.

In addition, these spiral garnets record strain rates at least an order magnitude faster than any directly measured by geochronological methods. This is consistent with the conclusion of Fagereng and Biggs (2019) that subduction and the development of young orogenic belts can produce high strains on time scales of several hundreds of thousands of years within faults or shear zones. In the rock we studied, the rapidly growing spiral garnet captures a critical pivot point marking the end of high-pressure metamorphism and shifting rapidly into incipient exhumation.

REFERENCES CITED

Aerden, D.G.A.M., and Ruiz-Fuentes, A., 2020, X-ray computed microtomography of spiral garnets: A new test of how they form: Journal of Structural Geology, v. 136, https://doi.org/10.1016/j.jsg.2020.104054.

Aerden, D.G.A.M., Bell, T.H., Puga, E., Sayab, M., Lozano, J.A., and de Federico, A.D., 2013, Multistage mountain building vs. relative plate motions in the Betic Cordillera deduced from integrated microstructural and petrological analysis of porphyroblast inclusion trails: Tectonophysics, v. 587, p. 188–206, https://doi.org/10.1016/j.tecto.2012.11.025.

Aerden, D.G.A.M., Farrell, T.P., Baxter, E.F., Stewart, E.M., Ruiz-Fuentes, A., and Bouybaouene, M., 2022, Refined tectonic evolution of the Betic-Rif orogen through integrated 3-D microstructural analysis and Sm-Nd dating of garnet porphyroblasts: Tectonics, v. 41, https://doi.org/10.1029/2022TC007366.

Baxter, E.F., and DePaolo, D.J., 2002, Field measurements of high temperature bulk reaction rates II: Interpretation of results from a field site near Simplon Pass, Switzerland: American Journal of Science, v. 302, p. 465–516, https://doi.org/10.2475/ajs.302.6.465.

Baxter, E.F., and DePaolo, D.J., 2004, Can metamorphic reactions proceed faster than bulk strain?: Contributions to Mineralogy and Petrology, v. 146, p. 657–670, https://doi.org/10.1007/s00410-003-0525-3.

Baxter, E.F., and Scherer, E.E., 2013, Garnet geochronology: Timekeeper of tectonometamorphic processes: Elements, v. 9, p. 433–438, https://doi.org/10.2113/gselements.9.6.433.

Bell, T.H., 1985, Deformation partitioning and porphyroblast rotation in metamorphic rocks: A radical reinterpretation: Journal of Metamorphic Geology, v. 3, p. 109–118, https://doi.org/10.1111/j.1525-1314.1985.tb00309.x.

Berg, C.A., Carlson, W.D., and Connelly, J.N., 2013, Strain rates at high temporal resolution from curved inclusion trails in garnet, Passo del Sole, Central Swiss Alps: Journal of Metamorphic Geology, v. 31, p. 243–262, https://doi.org/10.1111/jmg.12017.

Biermeier, C., and Stüwe, K., 2003, Strain-rate from snowball garnet: Journal of Metamorphic

Geology, v. 21, p. 253–268, https://doi.org/10.1046/j.1525-1314.2003.00441.x.

Christensen, J.N., Rosenfeld, J.L., and DePaolo, D.J., 1989, Rates of tectonometamorphic processes from rubidium and strontium isotopes in garnet: Science, v. 244, p. 1465–1469, https://doi.org/10.1126/science.244.4911.1465.

Christensen, J.N., Selverstone, J., Rosenfeld, J.L., and DePaolo, D.J., 1994, Correlation by Rb-Sr geochronology of garnet growth histories from different structural levels within the Tauern Window, eastern Alps: Contributions to Mineralogy and Petrology, v. 118, p. 1–12, https://doi.org/10.1007/BF00310607.

Dragovic, B., Baxter, E.F., and Caddick, M.J., 2015, Pulsed dehydration and garnet growth during subduction revealed by zoned garnet geochronology and thermodynamic modeling, Sifnos, Greece: Earth and Planetary Science Letters, v. 413, p. 111–122, https://doi.org/10.1016/j.epsl.2014.12.024.

Fagereng, Å., and Biggs, J., 2019, New perspectives on 'geological strain rates' calculated from both naturally deformed and actively deforming rocks: Journal of Structural Geology, v. 125, p. 100–110, https://doi.org/10.1016/j.jsg.2018.10.004.

Gatewood, M.P., Dragovic, B., Stowell, H.H., Baxter, E.F., Hirsch, D.M., and Bloom, R., 2015, Evaluating chemical equilibrium in metamorphic rocks using major element and Sm–Nd isotopic age zoning in garnet, Townshend Dam, Vermont, USA: Chemical Geology, v. 401, p. 151–168, https://doi.org/10.1016/j.chemgeo.2015.02.017.

Grujic, D., Warren, C.J., and Wooden, J.L., 2011, Rapid synconvergent exhumation of Miocene-aged lower orogenic crust in the eastern Himalaya: Lithosphere, v. 3, p. 346–366, https://doi.org/10.1130/L154.1.

Hayward, N., 1990, Determination of early fold axis orientations in multiply deformed rocks using porphyroblasts inclusion trails: Tectonophysics, v. 179, p. 353–369, https://doi.org/10.1016/0040-1951(90)90301-N.

Kirchner, K.L., Behr, W.M., Loewy, S., and Stockli, D.F., 2016, Early Miocene subduction in the western Mediterranean: Constraints from Rb-Sr multimineral isochron geochronology: Geochem-istry, Geophysics, Geosystems, v. 17, p. 1842–1860, https://doi.org/10.1002/2015GC006208.

Müller, W., Aerden, D.A.G.M., and Halliday, A.N., 2000, Isotropic dating of strain fringe increments: Duration and rates of deformation in shear zones: Science, v. 288, p. 2195–2198, https://doi.org/10.1126/science.288.5474.2195.

Pfiffner, O.A., and Ramsay, J.G., 1982, Constraints on geological strain rates: Arguments from finite strain rates of naturally deformed rocks: Journal of Geophysical Research, v. 87, p. 311–321, https://doi.org/10.1029/JB087iB01p00311.

Platt, J.P., Anczkiewicz, R., Soto, J.I., Kelley, S.P., and Thirwall, M., 2006, Early Miocene continental subduction and rapid exhumation in the western Mediterranean: Geology, v. 34, p. 981–984, https://doi.org/10.1130/G22801A.1.

Platt, J.P., Behr, W.M., Johanesen, K., and Williams, J.R., 2013, The Betic-Rif arc and its orogenic hinterland: A review: Annual Review of Earth and Planetary Sciences, v. 41, p. 313–357, https://doi.org/10.1146/annurev-earth-050212-123951.

Pollington, A.D., and Baxter, E.F., 2011, High precision microsampling and preparation of zoned garnet porphyroblasts for Sm–Nd geochronology: Chemical Geology, v. 281, p. 270–282, https://doi.org/10.1016/j.chemgeo.2010.12.014.

Puga, E., De Federico, A.D., and Nieto, J.M., 2002, Tectonostratigraphic subdivision and petrological characterization of the deepest complexes of the Betic Zone: A review: Geodinamica Acta, v. 15, p. 23–43, https://doi.org/10.1080/09853111.2002.10510737.

Puga, E., Fanning, M., Díaz-de-Federico, A., Nieto, J.M., Beccaluva, L., Bianchini, G., and Díaz Puga, M.A., 2011, Petrology, geochemistry and U–Pb geochronology of the Betic Ophiolites: Inferences for Pangaea break-up and birth of the westernmost Tethys Ocean: Lithos, v. 124, p. 255–272, https://doi.org/10.1016/j.lithos.2011.01.002.

Rosenfeld, J.L., 1968, Garnet rotations due to major Paleozoic deformations in southeast Vermont, *in* Zen, E., et al., eds., Studies of Appalachian Geology: New York, Interscience Publishers, p. 185–202.

Rubatto, D., and Hermann, J., 2001, Exhumation as fast as subduction?: Geology, v. 29, p. 3–6, https://doi.org/10.1130/0091-7613(2001)029<0003:EAFAS>2.0.CO;2.

Sánchez-Vizcaíno, V.L., Rubatto, D., Gómez-Pugnaire, M.T., Trommsdorff, V., and Müntener, O., 2001, Middle Miocene high-pressure metamorphism and fast exhumation of the Nevado-Filábride Complex, SE Spain: Terra Nova, v. 13, p. 327–332, https://doi.org/10.1046/j.1365-3121.2001.00354.x.

Santamaría-López, Á., Lanari, P., and de Galdeano, C.S., 2019, Deciphering the tectonometamorphic evolution of the Nevado-Filábride complex (Betic Cordillera, Spain)— A petrochronological study: Tectonophysics, v. 767, 128158, https://doi.org/10.1016/j.tecto.2019.06.028.

Smye, A.J., Greenwood, L.V., and Holland, T.J.B., 2010, Garnet-chloritoid-kyanite assemblages: Eclogite facies indicators of subduction constraints in orogenic belts: Journal of Metamorphic Geology, v. 28, p. 753–768, https://doi.org/10.1111/j.1525-1314.2010.00889.x.

Starr, P.G., Broadwell, K.S., Dragovic, B., Scambelluri, M., Haws, A.A., Caddick, M.J., Smye, A.S., and Baxter, E.F., 2020, The subduction and exhumation history of the Voltri Ophiolite, Italy: Evaluating exhumation mechanisms for high-pressure metamorphic massifs: Lithos, p. 376–377, https://doi.org/10.1016/j.lithos.2020.105767.

Tual, L., Smit, M.A., Cutts, J., Kooijman, E., Kielman-Schmitt, M., Majka, J., and Foulds, I., 2022, Rapid, paced metamorphism of blueschists (Syros, Greece) from laser-based zoned Lu-Hf garnet chronology and LA-ICPMS trace element mapping: Chemical Geology, v. 607, https://doi.org/10.1016/j.chemgeo.2022.121003.

Vance, D., and O'Nions, R.K., 1992, Prograde and retrograde thermal histories from the central Swiss Alps: Earth and Planetary Science Letters, v. 114, p. 113–129, https://doi.org/10.1016/0012-821X(92)90155-O.

Vermeesch, P., 2018, IsoplotR: A free and open toolbox for geochronology: Geoscience Frontiers, v. 9, p. 1479–1493, https://doi.org/10.1016/j.gsf.2018.04.001; corrigendum available at https://doi.org/10.1016/j.gsf.2021.101227.

Printed in the USA